Infrared Optical Properties of Nanoantenna Dimers with Photochemically Narrowed Gaps in the 5 nm Regime
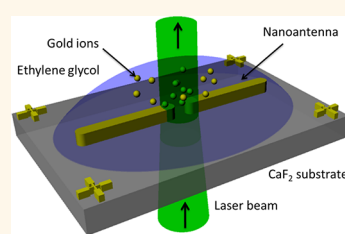
Frank Neubrech,[†,*] Daniel Weber,[†] Julia Katzmann,[‡] Christian Huck,[†] Andrea Toma,[§] Enzo Di Fabrizio,[§] Annemarie Pucci,[†] and Thomas Härtling[‡]

[†]Kirchhoff Institute for Physics, University of Heidelberg, Im Neuenheimer Feld 227, 69120 Heidelberg, Germany, [‡]Fraunhofer Institute for Nondestructive Testing, Maria-Reiche-Straße 2, 01109 Dresden, Germany, and [§]Nanostructures, Istituto Italiano di Tecnologia, Via Morego 30, 16163 Genova, Italy

Plasmonic nanostructures separated by gaps with sub-nanometer dimensions are of great interest in physics. For example, as a result of the sub-nanometer distance, nanogaps are well suited to serve as a model system for nonlocality[1] or quantum mechanical effects in plasmonics, such as tunneling.[2,3] Furthermore, nanoscale gaps of a few nanometers offer the possibility to enhance nonlinear signals[4] and carry great potential for the enhancement of spectroscopic signals of molecular species due to the strong confinement of electromagnetic fields. The application of such "hot spots" induced by localized surface plasmon polaritons was reported for surface-enhanced fluorescence,[5,6] surface-enhanced infrared absorption (SEIRA),[7,8] and surface-enhanced Raman spectroscopy (SERS)[9,10] in many different geometries. More recently, the extension of the experiments to nanoantenna-assisted SEIRA with nanostructures resonantly tuned to molecular infrared (IR) vibration bands was initiated, and attomolar sensitivity was achieved.[11−13] In comparison to conventional IR techniques, signal enhancements up to 500 000 accompanied by Fano-type line shapes (as a result of the electromagnetic coupling between the molecular and plasmonic excitation) were observed.[14] In agreement with theoretical simulations,[15,16] which predict an increased near-field and thus a tremendous increase in the IR signal,[17] it was found that nanoantennas separated by gaps of about 20 nm feature an increased molecular IR signal in comparison to individual structures.[18]

For all these aspects the challenge of large-scale and reproducible fabrication of nanostructures with suitable hot spots

ABSTRACT In this paper, we report on the manipulation of the near-field coupling in individual gold nanoantenna dimers resonant in the infrared (IR) spectral range. Photochemical metal deposition onto lithographically fabricated nanoantennas is used to decrease the gap between the antenna arms down to below 4 nm, as confirmed by finite-difference time-domain simulations. The increased plasmonic coupling in the gap region leads to a shift of the surface plasmon resonances to lower energies as well as to the appearance of hybridized plasmonic modes. All of the occurring electron oscillation modes can be explained by the plasmon hybridization model. Besides the bonding combination of the fundamental resonances of individual antennas, also the antibonding combination is observed in the IR transmittance at normal incidence. Its appearance is due to both structural defects and the small gaps between the antennas. The detailed analysis of individual IR antennas presented here allows a profound understanding of the spectral features occurring during the photochemical manipulation process and therefore paves the way to a full optical process monitoring of sub-nanometer scale gaps, which may serve as model systems for experimental studies of quantum mechanical effects in plasmonics.

KEYWORDS: plasmonics · nanoantennas · preparation of nanogaps · plasmon hybridization · infrared spectroscopy

remains. This is especially demanding in the case of nanoantenna-assisted SEIRA or terahertz applications, as structures in the micrometer range and hence resonant in the IR[19] or terahertz spectral range[20] have to be fabricated with gaps in the 10 nm regime. In a previous contribution we reported on the exploitation of photochemical metal deposition[21] to narrow the gaps sizes in IR nanoantennas on a flat substrate.[22] The spectral tuning of the antennas as well as the fabrication of interparticle gap sizes below 10 nm was successfully demonstrated with this approach. In that earlier work, the arrangement
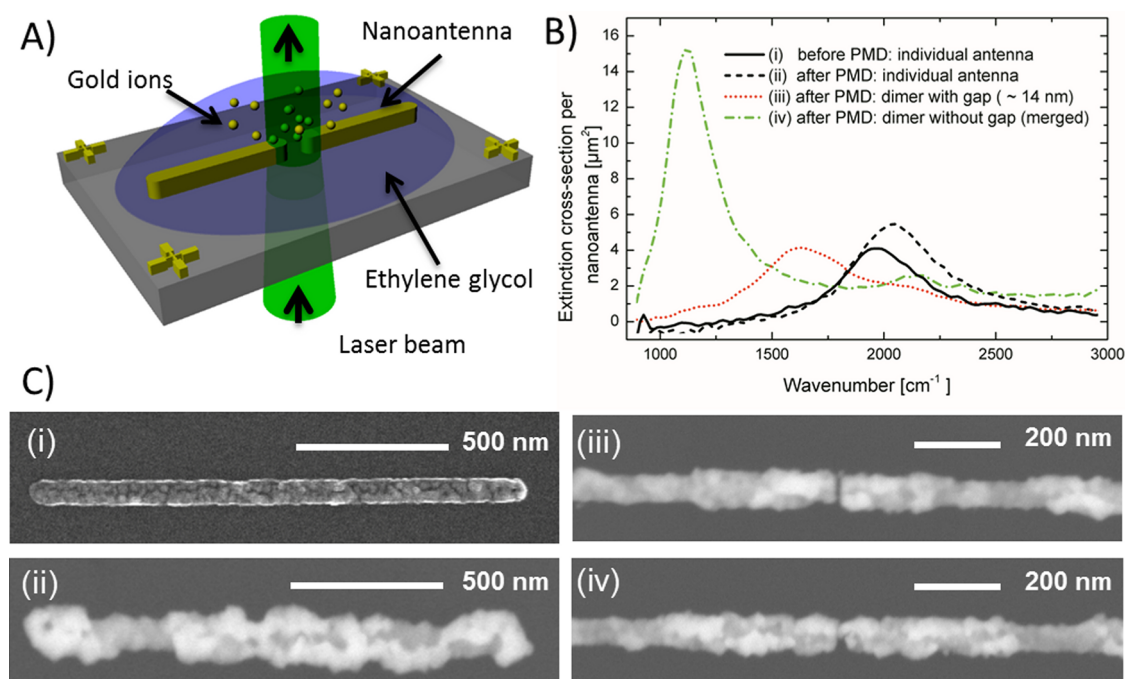
Figure 1. (A) Schematic illustration of photochemical metal deposition (PMD) on the lithographically prepared dimers. (B) Extinction cross-section per nanoantenna for an individual antenna, a dimer (consisting of two nanoantennas) featuring a narrow gap of 14 nm, and an already merged dimer with the corresponding representative SEM images shown in part C. (C) Individual nanoantennas before (i) and after (ii) PMD. (iii) Photochemically treated dimer with a gap of approximately 14 nm. (iv) Merged dimer. Note that the carbon layer cannot be seen in i—iv, since a material-specific backscattered electron detector was used.

of the nanoantennas in arrays and their parallel processing posed several difficulties. Especially the detailed analysis of the development of the spectral antenna properties during the tuning process was hampered by spectral broadening in the antenna ensemble. For example, no clear statement on the IR optical properties could be given for gaps below 10 nm. However, a profound understanding of the plasmonic modes and their spectral behavior is the key to a full control of the photochemical deposition process and its reliable application. We therefore extended our investigations to the photochemical tuning of *individual* nanoantenna pairs (dimers in the remainder of the text) consisting of two antenna arms (see Figure 1A for example). This approach allows us to follow the spectral changes of the occurring plasmonic antenna modes in detail and to clarify their origin. In particular, we observe an increased coupling between the antenna arms during the photochemical deposition process, which leads to a shift of the resonant excitations to lower energies as well as to the appearance of hybridized plasmonic modes. This behavior can be understood in the plasmon hybridization model,[23,24] as demonstrated by many researchers for various geometries (*e.g.*, rods, spheres, nanoshells, nanorings)[25] resonant in the visible spectral range. Besides the bonding combination of the resonant excitations of the individual antennas, also the antibonding combinations occur in our IR transmittance spectrum near normal incidence. We attribute their

appearance to both structural defects of the antennas[26] and the small gap size between the antennas as observed by optical spectroscopy[27−29] and electron energy loss studies.[31−33] The final gap sizes after photochemical deposition are estimated by a comparison with finite-difference time-domain (FDTD) simulations.

RESULTS AND DISCUSSION

Here we describe the plasmonic modes occurring in the IR spectra and discuss both their origin and their development during the metal deposition process in detail. In a first series of experiments, the photochemically prepared nanoantennas (dimers) were covered by a carbon layer to allow scanning electron microscopy (SEM) measurements. Afterward the carbon layer was removed by oxygen plasma cleaning and IR transmittance spectra were taken to correlate the structural information acquired by SEM imaging with the respective IR optical response.

In Figure 1B, selected IR extinction spectra (extinction cross-section per nanoantenna, see ref 26) and corresponding SEM images of individual nanoantennas before and after photochemical metal deposition as well as SEM images of nanoantenna dimers with and without a gap (merged dimers) are shown. In contrast to untreated nanoantennas, the photochemically modified antennas are very grainy. As recently reported,[22,34] this surface roughness plays only a minor role for the far-field optical properties of individual antennas.

For dimers with nanometer-sized gaps their optical far-field response may also depend on the roughness, since it determines the exact geometry at the point of closest separation. However, the near-field behavior of irregularly shaped particles, which is crucial for the signal enhancement in field-enhanced spectroscopic techniques, may considerably differ from that expected from regularly shaped antennas.[35]

A typical extinction cross-section of an untreated individual nanoantenna with its fundamental resonance at around 1900 cm^{-1} is shown in Figure 1. After photochemical deposition, we observe a shift of the extinction maximum to higher energies due to an increase of antenna width and height. This shift is in accordance with theory as well as the gain in extinction originating from the larger antenna volume.[36] Due to interaction, the resonance of the dimer with the nanometer-sized gap of approximately 14 nm is shifted to lower wavenumbers (frequencies) and features decreased far-field intensity.[16,37] This behavior can be explained with a simple coupled dipole model including retardation, where the frequency shift is interpreted as a result of lowered restoring forces.[16] Due to the linear relation between resonant wavelength and antenna length in the IR,[12,26,37] coalescence of the individual parts of the dimer (merged dimer) leads to a plasmonic resonance frequency at approximately half of the value of the individual antenna. Hence, IR spectroscopy might be used as a complementary tool to imaging techniques such as SEM or AFM for assessing supplementary information on the separation of nanoantenna dimers[38] and hence for monitoring the metal deposition process. In the present work we cannot provide such highly resolved SEM images in the limit of nanometer-separated antennas due to the limited lateral resolution of our SEM. Thus the gap size will be determined by a comparison of the measured optical response to FDTD simulations, as we will discuss later on.

In a second series of experiments, individual gold nanoantenna dimers were photochemically manipulated and IR spectroscopically investigated without being previously covered with a carbon layer. Figure 2A and B shows a selection of extinction spectra of a single nanoantenna and several nanoantenna dimers from this batch of samples. Each spectrum corresponds to a certain individual dimer, and the spectra are ordered corresponding to the resonance position of the fundamental resonance.

Due to inhomogeneous photochemical deposition (see Figure 1) and the limited lateral resolution of the available SEM, a precise determination of the gap sizes is not possible by means of electron microscopy. Nevertheless, information on the gap size can be obtained from the resonance frequency, since the shift of the resonance can be interpreted as a measure for the interantenna separation, as stated above. While an
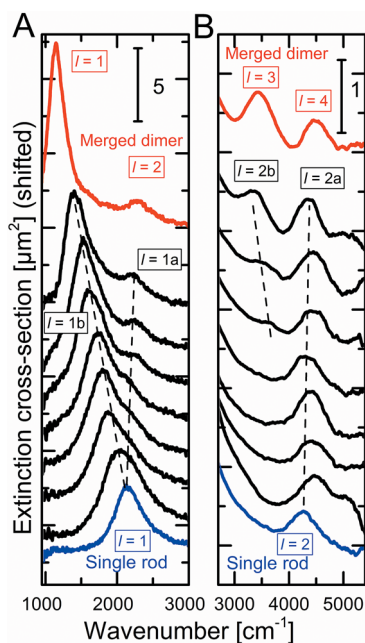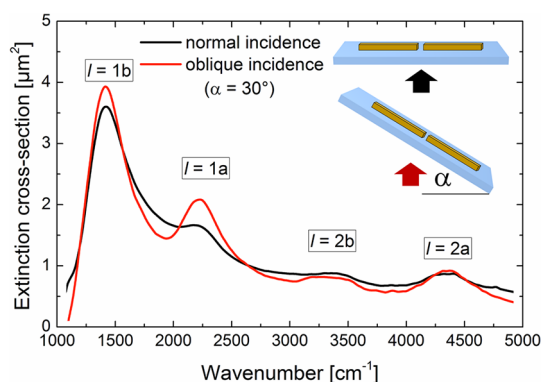

Figure 2. Extinction cross-section of an individual nanoantenna (blue), nanoantenna dimers with decreasing gap size (20 nm down to below 4 nm) from bottom to top (black), and a merged nanoantenna dimer (red). (A) Combinations of the $l = 1$ and (B) $l = 2$ modes of individual nanoantenna dimers. The mode notations "a" and "b" refer to the antibonding and bonding combinations, respectively (see also Figure 4). In part A, raw spectra are plotted, whereas in B, the spectra are smoothed using the Savitzky−Golay algorithm (200 points). An artificial vertical offset is used to provide clarity concerning the trend of mode shifting. The scale bars (in units of μm^2) in the upper right of the figure panels indicate the different signal strengths.

individual nanoantenna shows only one distinct resonance at around 2100 cm^{-1}, a second resonance emerges in the dimer spectra as the fundamental resonance shifts to smaller wavenumbers. IR spectra of such dimers taken under oblique incidence show an increased intensity of that second resonance, indicating a symmetric net dipole moment (see Figure 3). Thus, we attribute this second peak in the spectra to the antibonding combination of the $l = 1$ modes of the individual nanoantennas and refer to it as $l = 1a$ mode in contrast to the $l = 1b$ mode, which represents the bonding combination.

It is known that the $l = 1a$ mode can be excited when either the symmetry of the structure[26,29,39−41] or the symmetry of the excitation[42−45] is disturbed. In our case, a slight tilt of the sample and the nonperfect structure of the grown dimers (see SEM images in Figure 1C) are the reasons for symmetry breaking. In addition, only very small gap sizes below 20 nm lead to a sufficiently high energy splitting of the two modes.[30,41] Hence, the appearance of the $l = 1a$ mode suggests that the preparation of very small gaps was successful with the photochemical metal deposition technique.

A look at the high-energetic part of the spectra (Figure 2B) reveals that also the $l = 2$ mode of the

Figure 3. Extinction cross-section of a nanoantenna dimer with a gap size below 4 nm (as estimated from FDTD simulations (see Figure 4)) under normal incidence (black) and oblique ($\alpha = 30°$) incidence of light (red). As expected, the antibonding combinations ($l = 1a$ and $l = 2a$) are more pronounced for oblique measurements, indicating a symmetric net dipole moment.

individual antenna splits into two modes for sufficiently small gaps. This can be again explained by the formation of bonding and antibonding combinations of the individual antenna modes as proven by IR measurements under oblique incidence of light (see Figure 3). In contrast to the $l = 1$ modes, the $l = 2a$ mode reveals higher intensities with respect to the $l = 2b$ mode originating from its asymmetric excitation. However, in both cases ($l = 1$ and $l = 2$), the bonding combination is located at lower energies than the individual antenna mode since charges of opposite sign face each other in the gap region. In contrast, the antibonding modes appear at higher energies due to the repulsion of equal charges near the gap.[16]

In Figure 4 B, the idealized charge carrier distributions of the dimer modes are illustrated. The position of each mode is plotted *versus* the resonance frequency of the fundamental antenna resonance, which serves as an indirect measure of antenna separation.

Due to symmetry breaking, the supposedly dipole-inactive $l = 2a$ mode is always observed for nanoantenna dimers. Moreover, it is the phase relation between the individual antenna modes that determines their excitations. Only at very small gap sizes (large shifts of the fundamental resonance) can the antiphase mode $l = 2b$ be observed as a result of hybridization. The $l = 1a$ appears only for dimers (if hybridization takes place), and the symmetry is broken by either structural defects or oblique incidence.

When the two arms of the dimers merge, also four distinct peaks appear in the spectrum (see Figure 2). These resonances are attributed to the $l = 1-4$ modes with the respective charge carrier distributions illustrated in Figure 4. These modes can be considered as the border cases of the coupled dimer modes for vanishing gap size.[28,46,47] For the bonding modes, the opposite charges at the gap cancel out assuming flat rod ends. For arbitrary shapes of the rod ends, the situation depends on the nature of the contact point.
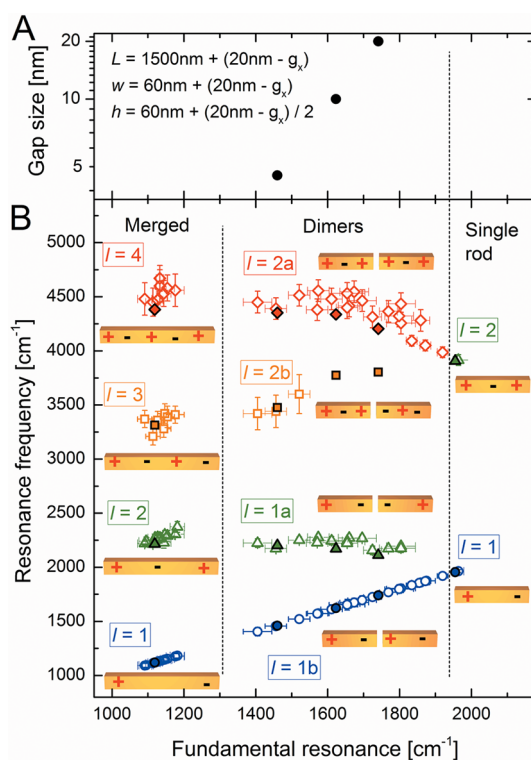
Figure 4. (A) Fundamental resonance position as obtained from FDTD simulations under oblique incidence ($\alpha = 20°$) of nanoantenna dimers with different gap sizes g_x. The modeling of homogeneous antenna growth in the simulations (see text) also requires a change of geometric antenna parameters as given in the legend. (B) Experimental (open symbols) and simulated (filled symbols with black border) resonance frequencies of all assigned modes ($l = 1-4$) of nanoantenna dimers with respect to the fundamental resonance position as a measure for separation. Therefore a straight line to the origin can be seen for the $l = 1b$ mode. The resonance frequency was chosen as the x-axis since no precise information on the gap size was available from SEM or AFM (see text). The idealized charge carrier distributions of the respective modes are indicated. Vertical dotted lines are used to provide clarity concerning different antenna types.

Finally, we carried out FDTD simulations (see methods) to estimate the final gap sizes after photochemical metal deposition. First, the transmittance of cuboid-shaped individual antennas with various lengths but fixed heights and widths ($w = h = 60$ nm) supported by a CaF_2 substrate was simulated and normalized to the transmittance of the bare substrate. The simulated transmittance was then compared to the experimental values of antennas before photochemical deposition. In this way, the antenna length most closely reproducing the experimental data was determined and selected for further simulations. Using nanoantennas with this length ($L = 1520$ nm), the growth of the antennas was modeled by increasing length, height, and width under the assumption of homogeneous deposition in all directions. Certainly, such a model does not include any kind of roughness or inhomogeneous growth. Nevertheless, since the roughness only marginally influences the IR optical far-field properties

of an individual antenna,[22,34,35] the spectral changes originating from photochemical deposition were reproduced within this simple model.

Also the IR spectral response of dimers with gap sizes down to 4 nm was simulated. Again, a homogeneous growth was taken as the basis, and thus also width, length, and height were changed for different gap sizes. Since the activation of antibonding modes needs some breaking of symmetry (either structural defects of the nanoantenna itself or oblique incidence; see for example Figure 3), we performed simulations using oblique illumination (α = 20). We found good agreement with the experimental data by comparing the extracted resonance frequencies of the respective modes from the simulated data (Figure 4 B). Furthermore, we plotted the fundamental resonance frequencies *versus* the gap size as shown in Figure 4A. As expected, the fundamental resonance shifts to lower frequencies for decreasing gap sizes due to interaction. On the basis of this relation we are now able to roughly estimate the experimentally prepared gap sizes: Evidently, gaps below 4 nm were successfully fabricated by photochemical metal deposition. As seen in Figure 4 even smaller gaps occur, but we refrain from further simulations with such small gaps due to computational and conceptual limitations (*e.g.*, simplified roughness of the antennas used in the simulations or nonlocal effects[49]). Especially the surface roughness may become a crucial point for narrower gaps, since the smallest distance between the antennas determines the optical response. We intend to study this effect in more detail in future investigations by varying the deposition parameters during the photoinduced chemical growth process.

SUMMARY AND CONCLUSION

With the above analysis, we are able to identify the origin of all plasmonic modes that occur during the photochemical treatment of the gold nanoantenna dimers and explain them by plasmon hybridization based on a simple coupled-dimer model. A comparison to FDTD simulations allows an estimation of gap sizes between the constituents of the dimers down to below 4 nm. The results demonstrate the possibility to exploit IR spectroscopy as a simple method for high-throughput and nondestructive monitoring of the photochemical deposition process and, in combination with FDTD simulations, to estimate gap sizes *in situ*. In particular, hybridized modes serve as indicators for very small gaps that are desired to obtain highly increased electric fields and accordingly enhanced optical signals.

These insights therefore pave the way to a cheap and reproducible fabrication of sub-nanometer-sized nanogaps in plasmonic structures, which may serve as a model system for experimental studies of theoretically predicted quantum mechanical effects in plasmonics such as tunneling induced by nanoscale gaps.[2,3] Furthermore, the experimental realization of nanometer-sized gaps as fabricated in the present study will enable the fabrication of new generation devices for ultrasensitive optical (bio)sensing.

METHODS

Individual gold nanoantenna dimers were fabricated by electron beam lithography (see below) and afterward modified by photochemical metal deposition. Since IR spectroscopic measurements during the metal deposition process are hindered by the IR absorption of the applied solvents, we conducted micro-IR spectroscopy before and after the deposition process. In addition to the fabrication of nanoantenna dimers also individual nanoantennas were prepared and treated in the same way in order to provide a reference. In the following the preparation steps and the micro-IR spectroscopic setup are described in detail.

Electron Beam Lithography. Nanoantennas and nanoantenna dimers were fabricated by means of electron beam lithography (Raith 150-Two). First, polymethyl methacrylate (MicroChem 950 PMMA A3) was spin-coated at 3000 rpm on a CaF$_2$ (100) substrate. A thin layer of aluminum was then deposited on the PMMA surface in order to avoid charging effects. Electron exposure was carried out at 20 keV beam energy and 450 μC/cm^2 exposure dose. After development in a conventional solution of MIBK/IPA (1:3) the nanostructures were deposited by electron beam evaporation of a 5 nm layer of titanium followed by 55 nm of gold. Subsequently, the unexposed resist was removed by lift-off in acetone. A representative image of an individual nanoantenna (typical initial length of L = 1490 nm and width of about 60 nm) was obtained by SEM, as shown in Figure 1. Before photochemical metal deposition the typical initial gap between the two arms of a nanoantenna dimer amounted to 20 nm.

Photochemical Metal Deposition. (See illustration in Figure 1A.) Photochemical metal deposition on the lithographically prepared nanoantennas and dimers was carried out following the description in ref 21. A droplet (volume of 20 μL) of 5 μM gold salt solution, produced by dissolving HAuCl$_4$ in ethylene glycol (99.9%), was pipetted on the antenna sample. Ethylene glycol was chosen as a solvent to avoid evaporation during the experiment as well as to provide optimal light transmission during exposure.

The sample covered with the gold salt solution was mounted onto an *xy*-piezo stage of an inverted optical microscope, and the deposition area was selected through the microscope eyepiece. Using the low-intensity white light beam of a mercury arc lamp (P = 10 μW), individual nanoantennas (dimers) were selected and brought into focus. After that, the white light beam was blocked and a frequency-doubled Nd:YAG-laser (λ = 532 nm) was directed into the microscope objective (100-fold magnification, NA = 0.75) by means of a flip mirror. Irradiation was performed with a slightly defocused spot (1 μm in the *z*-direction) to ensure illumination of the entire nanoantenna or dimer, respectively. The irradiation periods varied between 0.5 and 10 min at two defined laser powers (90 and 180 μW). Upon irradiation, gold ions are generated in the gold salt solution. Due to the catalytic effect of the gold antenna surface onto the reduction reaction, the ions are selectively deposited on the antennas. After illumination of the selected structure, the laser beam was blocked and another individual antenna or dimer was addressed and exposed to the laser radiation. After the photochemical treatment, the sample was rinsed with ethanol and dried by air purging.

Micro-IR Spectroscopy. Micro-IR spectroscopy of individual gold nanoantennas (dimers) was carried out using a commercial IR microscope (Bruker Hyperion 1000) coupled to a Fourier transform IR spectrometer (Bruker Tensor 27 with a LN_2-cooled mercury−cadmium−telluride detector, optical path purged with dried air). First, the position of an individual nanoantenna (dimers) was determined by means of white light microscopy. Then, we selected an area with a diameter of 16.7 μm (8.3 μm) in the focal plane using a circular aperture and centered it on an individual nanoantenna (dimer) for the IR transmission measurements. To account for a possible offset between the visible and IR optical beam path, systematic IR transmittance measurements at several positions close to the nanoantenna (dimer) were performed. After a normalization of the IR transmittance to a reference measurement, which was taken at least 30 μm away from the nanoantenna (dimer), the relative transmittance featuring the highest nanoantenna (dimer) signal was used for further analysis. All nanoantennas (dimers) were measured with a resolution of 32 cm^{-1} and 500 scans in the spectral range from 800 to 7000 cm^{-1}. Additionally, selected nanoantennas (dimers) were measured with a resolution of 4 cm^{-1} (8 cm^{-1}) and at least 40 000 scans to ensure a sufficient signal-to-noise ratio. An IR polarizer was inserted in the optical path before the sample to polarize the light along the long antenna axis.

FDTD Simulations. The simulations were performed by means of the FDTD software Lumerical and IR optical data by Palik.[48] In a first approximation, a numerical solution of the IR transmittance for individual nanoantennas and dimers was obtained by solving Maxwell's equations under oblique incidence. The antennas were placed at least one wavelength size away from the perfect matched layers (PMLs) in a finite space surrounded by 24 PMLs as boundary conditions. In order to resolve the nanometer-sized gap, subgridding techniques are used to obtain mesh cell resolutions down to $0.5 \times 0.5 \times 0.5$ nm^3 in the gap region. Mesh sizes with 5 nm in the largest dimension were chosen at the position of the nanoantenna (excluding the gap region) and mesh sizes smaller than 50 nm elsewhere. The structure is illuminated by a broadband Gaussian beam (centered at 2.5 μm wavelength) incident from a source placed inside the CaF_2 substrate with a Gaussian profile and electric field polarized along the long axis of the antenna. The transmission is calculated by integrating the power flux through a power monitor situated in air and normalizing it with respect to the source power. Convergence testing is performed by iteratively varying the number of PMLs and reducing the mesh volume until the results converge. At the end of the simulation (after 1500 fs of simulation time) we checked the decay of all fields and found a residual energy of below 1×10^{-3} of its peak value in the simulation volume.

Conflict of Interest: The authors declare no competing financial interest.

REFERENCES AND NOTES

1. Fernandez-Dominguez, A. I.; Wiener, A.; Garcia-Vidal, F. J.; Maier, S. A.; Pendry, J. B. Transformation-Optics Description of Nonlocal Effects in Plasmonic Nanostructures. *Phys. Rev. Lett.* **2012**, *108*, 106802.
2. Esteban, R.; Borisov, A. G.; Nordlander, P.; Aizpurua, J. Bridging Quantum and Classical Plasmonics with a Quantum-Corrected Model. *Nat. Commun.* **2012**, *3*, 825.
3. Marinica, D.; Kazansky, A.; Nordlander, P.; Aizpurua, J.; Borisov, A. G. Quantum Plasmonics: Nonlinear Effects in the Field Enhancement of a Plasmonic Nanoparticle Dimer. *Nano Lett.* **2012**, *12*, 1333–1339.3.
4. Schumacher, T.; Kratzer, K.; Molnar, D.; Hentschel, M.; Giessen, H.; Lippitz, M. Nanoantenna-Enhanced Ultrafast Nonlinear Spectroscopy of a Single Gold Nanoparticle. *Nat. Commun.* **2011**, *2*, 333.
5. Bardhan, R.; Grady, N. K.; Cole, J. R.; Joshi, A.; Halas, N. J. Fluorescence Enhancement by Au Nanostructures: Nanoshells and Nanorods. *ACS Nano* **2009**, *3*, 744–752.
6. Kinkhabwala, A.; Yu, Z.; Fan, S.; Avlasevich, Y.; Muellen, K.; Moerner, W. E. Large Single-Molecule Fluorescence Enhancements Produced by a Bowtie Nanoantenna. *Nat. Photonics* **2009**, *3*, 654–657.
7. Kundu, J.; Le, F.; Nordlander, P.; Halas, N. J. Surface Enhanced Infrared Absorption (SEIRA) Spectroscopy on Nanoshell Aggregate Substrates. *Chem. Phys. Lett.* **2008**, *452*, 115–119.
8. Wang, H.; Kundu, J.; Halas, N. J. Plasmonic Nanoshell Arrays Combine Surface-Enhanced Vibrational Spectroscopies on a Single Substrate. *Angew. Chem., Int. Ed.* **2007**, *46*, 9040–9044.
9. Theiss, J.; Pavaskar, P.; Echternach, P. M.; Muller, R. E.; Cronin, S. B. Plasmonic Nanoparticle Arrays with Nanometer Separation for High-Performance SERS Substrates. *Nano Lett.* **2010**, *10*, 2749–2754.
10. Nie, S.; Emory, S. R. Probing Single Molecules and Single Nanoparticles by Surface-Enhanced Raman Scattering. *Science* **1997**, *275*, 1102–1106.
11. Cataldo, S.; Zhao, J.; Neubrech, F.; Frank, B.; Zhang, C.; Braun, P. V.; Giessen, H. Hole-Mask Colloidal Nanolithography for Large-Area Low-Cost Metamaterials and Antenna-Assisted Surface Enhanced Infrared Absorption Substrates. *ACS Nano* **2012**, *6*, 979–985.
12. Adato, R.; Yanik, A. A.; Amsden, J. J.; Kaplan, D. L.; Omenetto, F. G.; Hong, M. K.; Erramilli, S.; Altug, H. Ultra-Sensitive Vibrational Spectroscopy of Protein Monolayers with Plasmonic Nanoantenna Arrays. *PNA* **2009**, *106*, 19227–19232.
13. Neubrech, F.; Cornelius, T. W.; Karim, S.; García-Etxarri, A.; Aizpurua, J.; Pucci, A. Resonant Plasmonic and Vibrational Coupling in a Tailored Nanoantenna for Infrared Detection. *Phys. Rev. Lett.* **2008**, *101*, 157403.
14. Giannini, V.; Francescato, Y.; Amrania, H.; Philips, C. C.; Maier, S. A. Fano Resonances in Nanoscale Plasmonic Systems: A Parameter-Free Modeling Approach. *Nano Lett.* **2011**, *11*, 2835–2840.
15. Pelton, M.; Aizpurua, J.; Bryant, G. Metal-Nanoparticle Plasmonics. *Laser Photonics Rev.* **2008**, *2*, 136–159.
16. Aizpurua, J.; Bryant, G. W.; Richter, L. J.; García de Abajo, F. J. Optical Properties of Coupled Metallic Nanorods for Field-Enhanced Spectroscopy. *Phys. Rev. B* **2005**, *71*, 235420.
17. Alonso-Gonzalez, P.; Albella, P.; Schnell, M.; Chen, J.; Huth, F.; Garcia-Etxarri, A.; Casanova, F.; Golmar, F.; Arzubiaga, L.; Hueso, L. E.; *et al*. Resolving the Electromagnetic Mechanism of Surface-Enhanced Light Scattering at Single Hot Spots. *Nat. Commun.* **2012**, *3*, 684.
18. Pucci, A.; F. Neubrech, F.; Weber, D.; Hong, S.; Toury, T.; Lamy de la Chapelle, M. Surface Enhanced Infrared Spectroscopy Using Gold Nanoantennas. *Phys. Status Solidi B* **2010**, *247*, 2071–2074.
19. Biagioni, P.; Huang, J.-S.; Hecht, B. Nanoantennas for Visible and Infrared Radiation. *Rep. Prog. Phys.* **2012**, *75*, 024402.
20. Razzari, L.; Toma, A.; Shalaby, M.; Clerici, M.; Zaccaria, R. P.; Liberale, C.; Marras, S.; Al-Naib, I. A. I.; Das, G.; De Angelis, F.; *et al*. Extremely Large Extinction Efficiency and Field Enhancement in Terahertz Resonant Dipole Nanoantennas. *Opt. Express* **2011**, *19*, 26088–26094.
21. Härtling, T.; Alaverdyan, Y.; Wenzel, M. T.; Kullock, R.; Käll, M.; Eng, L. M. Photochemical Tuning of Plasmon Resonances in Single Gold Nanoparticles. *J. Phys. Chem. C* **2008**, *112*, 4920–4924.
22. Weber, D.; Katzmann, J.; Neubrech, F.; Härtling, T.; Pucci, A. Spectral Tuning of Ir-Resonant Nanoantennas by Nanogap Engineering. *Opt. Mater. Express* **2011**, *1*, 1301–1306.

23. Prodan, E.; Radloff, C.; Halas, N. J.; Nordlander, P. A Hybridization Model for the Plasmon Response of Complex Nanostructures. *Science* **2003**, *302*, 419–422.

24. Nordlander, P.; Oubre, C.; Prodan, E.; Li, K.; Stockman, M. I. Plasmon Hybridization in Nanoparticle Dimers. *Nano Lett.* **2004**, *4*, 899–903.

25. Halas, N. J.; Lal, S.; Chang, W. S.; Link, S.; Nordlander, P. Plasmons in Strongly Coupled Metallic Nanostructures. *Chem. Rev.* **2011**, *111*, 3913–3961.

26. Neubrech, F.; Garcia-Etxarri, A.; Weber, D.; Bochterle, J.; Shen, H.; Lamy de la Chapelle, M.; Bryant, G. W.; Aizpurua, J.; Pucci, A. Defect-Induced Activation of Symmetry Forbidden Infrared Resonances in Individual Metallic Nanorods. *Appl. Phys. Lett.* **2010**, *96*, 213111.

27. Lassiter, J. B.; Aizpurua, J.; Hernandez, L. I.; Brandl, D. W.; Romero, I.; Lal, S.; Hafner, J. H.; Nordlander, P.; Halas, N. J. Close Encounters between Two Nanoshells. *Nano Lett.* **2008**, *8*, 1212–1218.

28. Romero, I.; Aizpurua, J.; Bryant, G. W.; García de Abajo, F. J. Plasmons in Nearly Touching Metallic Nanoparticles: Singular Response in the Limit of Touching Dimers. *Opt. Express* **2006**, *14*, 9988–9999.

29. Slaughter, L. S.; Wu, Y.; Willingham, B. A.; Nordlander, P.; Link, S. Effects of Symmetry Breaking and Conductive Contact on the Plasmon Coupling in Gold Nanorod Dimers. *ACS Nano* **2010**, *4*, 4657–4666.

30. Funston, A. M.; Novo, C.; Davis, T. J.; Mulvaney, P. Plasmon Coupling of Gold Nanorods at Short Distances and in Different Geometries. *Nano Lett.* **2009**, *9*, 1651–1658.

31. Koh, A. L.; Fernandez-Domanguez, A. I.; McComb, D. W.; Maier, S. A.; Yang, J. K. W. High-Resolution Mapping of Electron-Beam-Excited Plasmon Modes in Lithographically Defined Gold Nanostructures. *Nano Lett.* **2011**, *11*, 1323–1330.

32. Alber, I.; Sigle, W.; Möller, S.; Neumann, R.; Picht, O.; Rauber, M.; van Aken, P. A.; Toimil-Molares, M. E. Visualization of Multipolar Longitudinal and Transversal Surface Plasmon Modes in Nanowire Dimers. *ACS Nano* **2011**, *5*, 9845–9853.

33. Duan, H.; Fernandez-Domanguez, A. I.; Bosman, M.; Maier, S. A.; Yang, J. K. W. Nanoplasmonics: Classical Down to the Nanometer Scale. *Nano Lett.* **2012**, *12*, 1683–1689.

34. Trügler, A.; Tinguely, J.-C.; Krenn, J. R.; Hohenau, A.; Hohenester, U. Influence of Surface Roughness on the Optical Properties of Plasmonic Nanoparticles. *Phys. Rev. B* **2011**, *83*, 081412.

35. Kern, A. M.; Martin, O. J. F. Excitation and Reemission of Molecules Near Realistic Plasmonic Nanostructures. *Nano Lett.* **2011**, *11*, 482–487.

36. Fromm, D. P.; Sundaramurthy, A.; Schuck, P. J.; Kino, G.; Moerner, W. E. Gap-Dependent Optical Coupling of Single Bowtie Nanoantennas Resonant in the Visible. *Nano Lett.* **2004**, *4*, 957–961.

37. Weber, D.; Albella, P.; Alonso-González, P.; Neubrech, F.; Han, G.; Nagao, T.; Hillenbrand, R.; Aizpurua, J.; Pucci, A. Longitudinal and Transverse Coupling in Infrared Gold Nanoantenna Arrays: Long Range *versus* Short Range Interaction Regimes. *Opt. Express* **2011**, *19*, 15047–15061.

38. Han, G.; Weber, D.; Neubrech, F.; Yamada, I.; Mitome, M.; Bando, Y.; Pucci, A.; Nagao, T. Infrared Spectroscopic and Electron Microscopic Characterization of Gold Nanogap Structure Fabricated by Focused Ion Beam. *Nanotechnology* **2011**, *22*, 275202.

39. Wang, H.; Halas, N. J. Plasmonic Nanoparticle Heterodimers in a Semiembedded Geometry Fabricated by Stepwise Upright Assembly. *Nano Lett.* **2006**, *6*, 2945–2948.

40. Hao, F.; Sonnefraud, Y.; Van Dorpe, P.; Maier, S. A.; Halas, N. J.; Nordlander, P. Symmetry Breaking in Plasmonic Nanocavities: Subradiant LSPR Sensing and a Tunable Fano Resonance. *Nano Lett.* **2008**, *8*, 3983–3988.

41. Huang, J. S.; Kern, J.; Geisler, P.; Weinmann, P.; Kamp, M.; Forchel, A.; Biagioni, P.; Hecht, B. Mode Imaging and Selection in Strongly Coupled Nanoantennas. *Nano Lett.* **2010**, *10*, 2105–2110.

42. Yang, H.; Kobori, S.-C.; He, C.-L.; Lin, M.-H.; Chen, H.-Y.; Li, C.; Kanehara, M.; Teranishi, T.; Gwo, S. Plasmon Hybridization in Individual Gold Nanocrystal Dimers: Direct Observation of Bright and Dark Modes. *Nano Lett.* **2010**, *10*, 632–637.

43. Chu, M.-W.; Myroshnychenko, V.; Chen, C. H.; Deng, J. P.; Mou, F. J.; García de Abajo, C.-Y. Probing Bright and Dark Surface-Plasmon Modes in Individual and Coupled Noble Metal Nanoparticles Using an Electron Beam. *Nano Lett.* **2009**, *9*, 399–404.

44. Volpe, G.; Cherukulappurath, S.; Parramon, R. J.; Molina-Terriza, G.; Quidant, R. Controlling the Optical Near Field of Nanoantennas with Spatial Phase-Shaped Beams. *Nano Lett.* **2009**, *9*, 3608–3611.

45. Koh, A. L.; Bao, K.; Khan, I.; Smith, W. E.; Kothleitner, G.; Nordlander, P.; Maier, S. A.; McComb, D. W. Electron Energy-Loss Spectroscopy (EELS) of Surface Plasmons in Single Silver Nanoparticles and Dimers: Influence of Beam Damage and Mapping of Dark Modes. *ACS Nano* **2009**, *3*, 3015–3022.

46. Perez-Gonzalez, O.; Zabala, N.; Borisov, A. G.; Halas, N. J.; Nordlander, P.; Aizpurua, J. Optical Spectroscopy of Conductive Junctions in Plasmonic Cavities. *Nano Lett.* **2010**, *10*, 3090–3095.

47. Schnell, M.; Garcia-Etxarri, A.; Alkorta, J.; Crozier, K.; Aizpurua, J.; Hillenbrand, R. Controlling the Near-Field Oscillations of Loaded Plasmonic Nanoantennas. *Nat. Photonics* **2009**, *3*, 287–291.

48. Palik, E. D. *Handbook of Optical Constants of Solids*; Academic: New York, 1985.

49. McMahon, J. M.; Gray, S. K.; Schatz, G. C. Optical Properties of Nanowire Dimers with a Spatially Nonlocal Dielectric Function. *Nano Lett.* **2010**, *10*, 3473–3481.